Published online 7 April 2011 *Nucleic Acids Research, 2011, Vol. 39, No. 14* ***5955–5966***
doi:10.1093/nar/gkr196

Efficient mutagenesis of the rhodopsin gene in rod photoreceptor neurons in mice

Fung Chan[1], William W. Hauswirth[2], Theodore G. Wensel[1] and John H. Wilson[1,*]

[1]Verna and Marrs McLean Department of Biochemistry and Molecular Biology, Baylor College of Medicine, Houston, TX 77030 and [2]Department of Ophthalmology, University of Florida, Gainesville, FL 32610, USA

Received January 12, 2011; Revised February 24, 2011; Accepted March 17, 2011

ABSTRACT

Dominant mutations in the rhodopsin gene, which is expressed in rod photoreceptor cells, are a major cause of the hereditary-blinding disease, autosomal dominant retinitis pigmentosa. Therapeutic strategies designed to edit such mutations will likely depend on the introduction of double-strand breaks and their subsequent repair by homologous recombination or non-homologous end joining. At present, the break repair capabilities of mature neurons, in general, and rod cells, in particular, are undefined. To detect break repair, we generated mice that carry a modified human rhodopsin-GFP fusion gene at the normal mouse rhodopsin locus. The rhodopsin-GFP gene carries tandem copies of exon 2, with an ISceI recognition site situated between them. An ISceI-induced break can be repaired either by non-homologous end joining or by recombination between the duplicated segments, generating a functional rhodopsin-GFP gene. We introduced breaks using recombinant adeno-associated virus to transduce the gene encoding ISceI nuclease. We found that virtually 100% of transduced rod cells were mutated at the ISceI site, with ~85% of the genomes altered by end joining and ~15% by the single-strand annealing pathway of homologous recombination. These studies establish that the genomes of terminally differentiated rod cells can be efficiently edited in living organisms.

INTRODUCTION

Defects in the rhodopsin gene cause the most common form of the most common hereditary blinding disease, retinitis pigmentosa (RP) (1,2). RP is a progressive neurodegenerative disorder that begins with the death of rod photoreceptors, where rhodopsin is expressed, but ultimately destroys rod and cone cells, leading to loss of both dim-light and color vision. All but a handful of the more than 100 rhodopsin alleles that cause retinal degeneration display dominant inheritance (1,2). It is clear that dominance arises from the harmful effects of mutant rhodopsin, rather than from a lack of adequate protein levels, since human patients heterozygous for rare, null alleles of the rhodopsin gene and mice with one knockout allele do not suffer from serious degeneration (3–5). Thus, it is the presence of rhodopsin encoded by the dominant allele that leads to degeneration, although it remains an open question whether its deleterious consequences are due to toxic gain-of-function or interfering dominant-negative effects (6). In either case, correcting the defective allele, or knocking it out, would be expected to preserve retinal function by diminishing the loss of rod cells, which in turn would protect cones and extend the useful lifetime of central vision.

A promising general strategy for editing the genome in living cells is to introduce a double-strand break (DSB) into the target gene and exploit the normal cellular DSB repair processes to bring about the desired change (7–11). Repair of the break by homologous recombination (HR), in the presence of a non-mutant segment of DNA to act as the template for repair, can correct the mutation (11). Alternatively, repair by non-homologous end joining (NHEJ), which is usually mutagenic, can knockout gene expression (12). Although HR and NHEJ have been well-defined in cycling mammalian cells (13), their characterization in mature neurons, which no longer divide, is in its infancy (14). At present, it is uncertain whether terminally differentiated rod photoreceptor neurons possess the requisite capabilities for DSB-dependent genome editing.

It is clear that the developing nervous system is exquisitely sensitive to DSBs, and that DSB repair by HR and NHEJ is critical to prevent cell death by apoptosis (15). Defects in either repair pathway, or the signaling pathways that control them, can lead to neurological defects and disease in humans and mouse models (15–17). For example, mutations in the ATM gene in humans lead to defects in the signaling response to DSBs, which causes

*To whom correspondence should be addressed. Tel: +713 798 5760; Fax: +713 796 9438; Email: jwilson@bcm.edu

ataxia telangiectasia, a progressive neurodegenerative disease that compromises the function of the cerebellum. Although HR and NHEJ play important roles in the proliferation and early stages of differentiation of the nervous system, their contribution to genome maintenance in the mature nervous system is poorly defined (14). Because terminally differentiated, non-dividing nerve cells in the brain are mixed with a comparable number of glial cells that retain mitotic capability, analysis of DSB repair in neurons is inherently challenging. However, extracts from unfractionated and neuron-enriched rat brain samples display NHEJ activity, which declines with age (18,19). These studies suggest that the NHEJ pathway of DSB repair is probably functional in mature neurons.

Studies in cycling cells, the source of virtually all our detailed information on DSB repair in mammalian cells, indicate that HR functions primarily in the S and G2 phases of the cell cycle, when a sister chromatid—the preferred template for HR repair—is available (20–22). Since neurons are trapped in G1/G0, it is unclear *a priori* whether HR is a viable strategy for modifying the rhodopsin gene in rod photoreceptors. The block to HR in G1 in cycling cells appears to be enforced at the step of 5′ to 3′ resection of the ends, which is required to expose the single-stranded DNA needed for the strand-invasion step in HR (23–25). In contrast, end resection is not needed for NHEJ, which operates throughout the cell cycle (13,20–22).

These considerations led us to expect that DSBs in rod photoreceptor cells would likely be repaired predominantly by mutagenic NHEJ and rarely, if at all, by HR. Thus, we designed a mouse model that would allow us to detect common NHEJ events by PCR-based methods and rare HR events by an exquisitely sensitive fluorescent assay that is capable of providing a reliable readout for one or a few events per retina (26,27). To detect HR repair of DSBs, we replaced one mouse rhodopsin gene with a modified form of the human rhodopsin gene fused to enhanced GFP (26). This modified rhodopsin-GFP gene carries two copies of exon 2, which flank the recognition sequence for the rare-cutting nuclease, ISceI. The duplicate copy of exon 2 shifts the reading frame so that rhodopsin-GFP is not expressed. Break-induced recombination between the duplicated segments will reconstitute a functional rhodopsin-GFP gene, giving rise to a bright fluorescent green outer segment on each corrected rod cell. This recombination substrate is expected to generate green rods by the single-strand annealing (SSA) pathway of HR. SSA, like the Rad51-mediated strand-invasion pathway of HR, begins by resection of ends at a DSB, but completes the repair event by pairing the exposed, single strands at complementary regions, thereby bypassing strand invasion. Thus, by assaying for the SSA pathway of HR, this duplication substrate tests whether end resection occurs during DSB repair in rod cells, which is a prerequisite for genome editing by HR.

Using recombinant adeno-associated virus (rAAV) to introduce the ISceI gene, we addressed three questions about DSBs in terminally differentiated rod photoreceptor neurons. Can DSBs be efficiently introduced into the rhodopsin gene? Can NHEJ and SSA repair DSBs in rod cells? And if so, what are their relative frequencies? Here, we show that most, if not all, rAAV-transduced rod cells were cleaved at the target site, with 85% of the DSBs repaired by NHEJ and 15% by SSA. The high frequency of DSB repair by mutagenic NHEJ lays the foundation for plausible therapeutic strategies designed to treat RP by knocking out dominant rhodopsin alleles in rod cells in patients. The surprisingly high frequency of DSB repair by SSA indicates that end resection is unlikely to block HR in rod cell neurons, raising the possibility that correction of mutant rhodopsin alleles by HR may also be achievable. Collectively, these results establish that the genomes of terminally differentiated rod photoreceptor neurons can be efficiently edited in living organisms.

MATERIALS AND METHODS

Generation of ID2-hRho-GFP knockin mice

All animal procedures were carried out according to protocols approved by the Baylor College of Medicine Institutional Animal Care and Use Committee, and in accordance with the Statement for the Use of Animals in Ophthalmic and Visual Research of the Association for Research in Vision and Ophthalmology. Knockin mice were generated by gene targeting in HPRT-negative embryonic stem (ES) cells. To make the targeting vector, we modified a previously described segmental replacement vector (26), which carried the human rhodopsin-GFP fusion gene flanked by LoxP and Lox511 sites, by inserting a duplicate copy of exon 2 generated by PCR. The PCR amplified segment comprised 613 bp of rhodopsin sequences, which included exon 2 along with 282 bp and 162 bp of 5′- and 3′-flanking sequences, respectively, and carried an EcoRV site and an ISceI site at its 5′-end and an EcoRV site at its 3′-end. We inserted this PCR segment 706-bp downstream of the endogenous exon 2 into an artificial EcoRV site that was made by point mutation (AATATC to GATATC) to generate the ID2-hRho-GFP gene. To construct the gene-targeting vector, we excised the 8-kb ID2-hRho-GFP gene from its plasmid by NotI digestion and cloned it into the NotI site at 3′-end of the HPRT minigene in the first-step targeting vector described previously (26). This cloning step generates a vector that contains the ID2-hRho-GFP gene adjacent to a LoxP-flanked HPRT minigene, with 4.1 kb of upstream and 6.5 kb of downstream sequences from the mouse rhodopsin locus (Figure 1A). We attached the herpes virus TK gene to one end of the construct to allow selection against random integrants. The targeting vector contains a pBluescriptSK plasmid backbone.

We modified the rhodopsin locus in the HPRT-negative ES cell line AB2.2 123, which was derived from mouse strain 129SvEv, by HR so that the endogenous mouse rhodopsin gene was replaced by an 11.9-kb Sac1–HindIII fragment containing the LoxP-flanked HPRT minigene linked to the ID2-hRho-GFP gene (Figure 1A). The Darwin Transgenic Core Facility, Baylor College of Medicine, electroporated ES cells in the presence of 15 μg linearized targeting vector, and grew the treated cells on mitomycin C inactivated SNLP

76/7-4 Puro feeder cells. Selection for $HPRT^{+}TK^{-}$ cells was applied after 24 h by growth in HAT medium (0.1 mM hypoxanthine/0.4 μM aminopterin/16 μM thymidine) plus 0.2 μM 1-(2-deoxy-2-fluoro-1-D-arabinofuranosyl)-5-iodouracil (FIAU) for 7 days, followed by growth in HT medium (0.1 mM hypoxanthine/16 μM thymidine) for 4 days.

We screened colonies that survived selection by Southern blotting after DNA from individual colonies had been digested with a restriction enzyme (BamHI for the 5′-end and HindIII for the 3′-end), electrophoresed on 0.7% agarose gels, and blotted onto Nylon membranes (Hybond-N^{+}, Amersham Biosciences). To identify correctly targeted clones at the 5′-end, we probed blots with the 1.1-kb BamHI–SacI mouse genomic fragment upstream of the 5′-flanking homology used in the targeting vectors. For the 3′-end, we used a 1.0-kb BglII–EcoRI DNA probe, which is a subfragment of the 6.5-kb 3′-flanking homology used in the targeting vector. All probes were labeled by random priming in the presence of α-^{32}P-dCTP (Megaprime DNA labeling system, Amersham Biosciences).

The Darwin Transgenic Core injected modified ES cells into blastocysts from albino C57BL/6-$Tyr^{c\text{-}Brd}$ mice (28). We then tested chimeric males for germline transmission by crossing them with C57BL/6-$Tyr^{c\text{-}Brd}$ mice and observing coat color and genotyping by PCR (Figure 1C). We generated homozygous HPRT-ID2-hRho-GFP (HPRT-ID2) mice by crossing F1 progeny. We removed the HPRT minigene in two steps. By crossing appropriate mice, we combined the HPRT-ID2 allele with a transgene (GDF-9-iCre) that expresses iCre from the GDF-9 promoter, which drives expression in the female germline (29). Mice expressing the transgene were a gift from Dr Austin J. Cooney. We then bred female HPRT-ID2/GDF-9-iCre mice to wild-type C57Bl/6 mice to generate mice that had eliminated the HPRT minigene. PCR analysis of progeny identified ID2-hRho-GFP mice that were missing the HPRT minigene and the GDF-9-iCre transgene (Figure 1E, pup 4).

See Supplementary Data for details of mouse genotyping and histology.

AAV-ISceI vector construction and subretinal injection

The rAAV-ISceI carries AAV2 inverted terminal repeats in pseudotyped AAV5 capsids and expresses ISceI from the proximal murine rod opsin promoter (from −385 to +86), which drives expression of the recombinant gene product almost exclusively in photoreceptors (30). We built the plasmid precursor of rAAV-ISceI using the pTR-MOPS500(E-)GFP vector (30). We began by inserting a double-stranded oligonucleotide (5′-NotI–EcoRI–BamHI–SalI) in place of the multicloning sites between the NotI and SalI sites in phagemid pBlueScript SKII. We used EcoRI and BamHI to excise a 0.87-kb fragment containing the ISceI transcription unit with the 3x nuclear localization signal from plasmid pCMV-3x nls-ISceI (7), and subcloned it into the modified pBlueScript SKII vector. We then digested the resulting construct with NotI and SalI to liberate the ISceI fragment and inserted it into the pTR-MOPS500(E-)GFP vector in place of the existing 1.3-kb NotI–SalI fragment that encoded EGFP. We used the resulting pTR-MOPS500-ISceI vector to generate rAAV-ISceI (2.25×10^{12} viral particles per milliliter) by standard procedures (30). The pTR-MOPS500(E-)GFP vector was used to generate rAAV-GFP (1.38×10^{14} viral particles per milliliter).

For subretinal injections, we followed established procedures (31) with some modification (Supplementary Data). We performed subretinal injections under direct observation via a dissecting microscope (SMZ-800 Zoom Stero Microscope, Nikon Instruments Inc.) at ×30 magnification. We injected ~0.7 μl to 1 μl of rAAV-GFP or rAAV-ISceI subretinally using UltraMicroPump II (World Precision Instruments) for mice of 8–12g. After all injections, we treated mice daily with 1% atropine eye drops and neomycin/polymyxin B/bacitracin ophthalmic ointments for 3 days. At 4–27 weeks post-injection, we prepared retinal whole mounts for examination.

Fluorescence microscopy

Retinal whole mounts were prepared 4–27 weeks after injection from eyes fixed in 4% paraformaldehyde, by removing the cornea, lens and vitreous and dissecting the retina from the eyecup. We placed the retina on a slide with the photoreceptors up, flattened it by making radial incisions, and mounted it with Gel/Mount (Biomeda, Foster City, CA, USA). To determine the frequency of fluorescent green rods, we captured multiple images from each injected retina using an LSM 510 laser-scanning confocal microscope (Zeiss). The affected areas of retinas, as judged by the presence of green rods, ranged from <5% to >80% of the overall retina in different samples; however, we quantified green rods only in the transduced areas. For rAAV-GFP-injected controls, we collected one retina for each time point, except the 4-week sample, for which we collected two. For rAAV-ISceI injected mice, we examined 2–5 retinas for the 6-, 7-, 8-, 10- and 12-week time points and one retina each for the 4-, 5-, 18-, 19-, 24-, 26- and 27-week time points. We examined retinas using either a ×40 or a ×63 objective and a ×10 eyepiece. We manually counted all the green rods in a 50 μm × 50 μm area of the ×63 image or in the entire 230 μm × 230 μm field of the ×40 image. We counted several different fields for each retina, adjusted the counts to the area of the ×40 image and averaged them.

PCR analysis of DSB-repair events

We designed nested sets of primers to detect the products of SSA and NHEJ. Primer sites and product sizes are shown schematically in Figure 3A (see Supplementary Data for primer sequences). PCR analysis of SSA and NHEJ products in bulk samples is given in Supplementary Data. For small-pool PCR analysis, we isolated DNA from retinal whole mounts that had been examined by confocal microscopy and shown to have a substantial proportion of fluorescent green rods. Slides were washed in 1× PBS for 10 min to loosen the cover slip, and the mounted retinas were scooped up with a

razor blade and washed several times to remove mounting media. We extracted DNA from the recovered retinas using the same protocol for isolating tail DNA. We treated individual retinas with 250 μg of proteinase K in 500 μl of lysis buffer containing 50 mM Tris, pH 7.5, 50 mM EDTA, pH 8.0, 100 mM NaCl, 5 mM DTT, 0.5 mM spermidine and 1% SDS at 55°C overnight with constant agitation. The lysate was then extracted once with phenol–chloroform–isoamyl alcohol (25:24:1), and the high-molecular weight DNA was precipitated and spooled out by adding 0.15 volumes of 7.5 M NH_4OAc and three volumes of absolute alcohol. The DNA was rinsed successively in 70% alcohol and 100% alcohol, and then air-dried and dissolved in 250 μl TE.

To eliminate unmodified genomes from the analysis, we digested 5 μg of retinal DNA at 37°C with 30 units of ISceI endonuclease for 3 h, and then added 30 more units of enzyme and digested the sample overnight. We then extracted the digestion mixture once with phenol–chloroform–isoamyl alcohol, precipitated it with alcohol, and dissolved the pellet in TE. We then repeated this ISceI-digestion protocol once more. Finally, we digested this DNA with BamH1, which does not cleave within the amplified region, to reduce viscosity and maintain consistency during serial dilutions.

For small-pool PCR, we initially set up seven reactions each at DNA concentrations of 100, 50, 25 and 12.5 pg per reaction in order to determine the optimum dilution to use for each retina, so that each reaction contained less than two amplifiable genomes on average. We used a mixture of three PCR primers, two forward primers (P1 and P6) and a reverse primer (P2), to amplify genomes repaired by SSA and NHEJ (Figure 3A). Primers P1 and P2 yield a 687-bp band for SSA products; primers P6 and P2 yield a variety of bands near 997 bp for NHEJ products, depending on the extent of modification at the repaired junction. Primers P1 and P2 could potentially generate a 1.8-kb band from NHEJ products, but we selected PCR conditions that were not favorable for this long product. We used Roche's Expand Long Template PCR System (Roche, Cat. No. 11 681 842 001) with buffer 2, 1.25 U of enzyme, 0.54 mM dNTPs and 0.63 μM for each primer, in a final reaction volume of 15 μl. The PCR program was 94°C for 2 min for initial denaturation, followed by 15 cycles of 94°C for 10 s, 60°C for 30 s, 68°C for 45 s, then another 15 cycles with 1 s extra extension time per each additional cycle, and one final cycle at 68°C for 7 min. We divided the PCR products into two portions: one for small-pool PCR analysis and the second for follow-up ISceI digestions. For small-pool PCR analysis, samples were separated by electrophoresis on 1.5% TAE agarose gels at 25 V for 18 h, transferred to a 0.45-μm nylon membrane (Magnaprobe, GE Water & Process Technologies), and hybridized with α-^{32}P-dCTP labeled 687-bp PCR DNA, which was generated using primer P1 and P2 to amplify the 687-bp band from plasmid pCR2.1-TOPO-687, which carried the SSA product. The positions of bands were visualized by phosphorimaging.

To determine whether bands near the 997-bp marker arose by amplification of an NHEJ product or a genome with an intact ISceI site, we re-amplified the portion of the sample we had set aside, using the same conditions as before, except in a 50-μl reaction volume and using 25 cycles of amplification in the second step of PCR using the nested primers P8/P3. We then digested the amplified material with ISceI, which would cut an intact genome into 312- and 644-bp fragments. Cutting was assessed by electrophoresis on an agarose gel.

Analysis of individual green rods

We collected retinas from ID2-hRho-GFP mice injected with AAV-ISceI 7–8 weeks post-injection, and dissociated them using a modification of a previously described protocol (32). In brief, we pooled 2–3 injected retinas and incubated them for a short time in a pronase solution at 37°C. We dissociated the pronase-treated retinas at room temperature by two cycles of 50 passages through a 1-ml pipette tip, pelleting of the retinal fragments by centrifugation, and removal of the supernatant for the next cycle of treatment. About 0.5 ml of the combined cell suspensions was spread over a 50-mm glass bottom dish (MatTek Corporation). We picked individual green rods under the fluorescent microscope (Nikon Eclipse TE2000-U), using a motorized micromanipulator system (MP-225, Sutter Instrument) and a micropipette with a 5–6 μm inner diameter and 30-degree bend at the tip (Origio Humagen Pipets). We then ejected the picked green rod into a 100-μl PCR tube (Applied Biosystems) containing 2 μl of denaturing reagents. Rhodopsin cDNA was prepared using the QIAGEN OneStep RT-PCR kit. We amplified the cDNA using primers to GFP and exon 1 of human rhodopsin. The initial product was further amplified using nested primers within GFP and exon 1. Products were analyzed by gel electrophoresis, with bands at 960 bp indicating mRNAs with two copies of exon 2 and bands at 791 bp indicating mRNAs with one copy of exon 2, consistent with SSA. We sequenced the bands to verify their structure. A detailed description of this protocol is included in Supplementary Data.

RESULTS

The ID2-hRho-GFP mouse model

We generated mice carrying a human rhodopsin-GFP fusion gene with a duplicated copy of exon 2 (ID2-hRho-GFP) by homologous replacement of the endogenous mouse rhodopsin gene in a two-step procedure, as outlined in Figure 1A. The targeting construct carries a modified version of the human rhodopsin gene linked to the sequences that flank the mouse rhodopsin gene. We modified the genomic human rhodopsin gene in three ways. First, we fused the gene for enhanced GFP to the C-terminus of the rhodopsin gene, so that the encoded rhodopsin protein would be linked to GFP through the peptide APVAT, as described previously (26). Second, we inserted a 613-bp segment encompassing exon 2 into intron 2 to create an internal duplication, with the two segments separated by 564 bp that include the recognition site for the rare-cutting nuclease ISceI. The predicted splicing pattern for the modified rhodopsin gene would

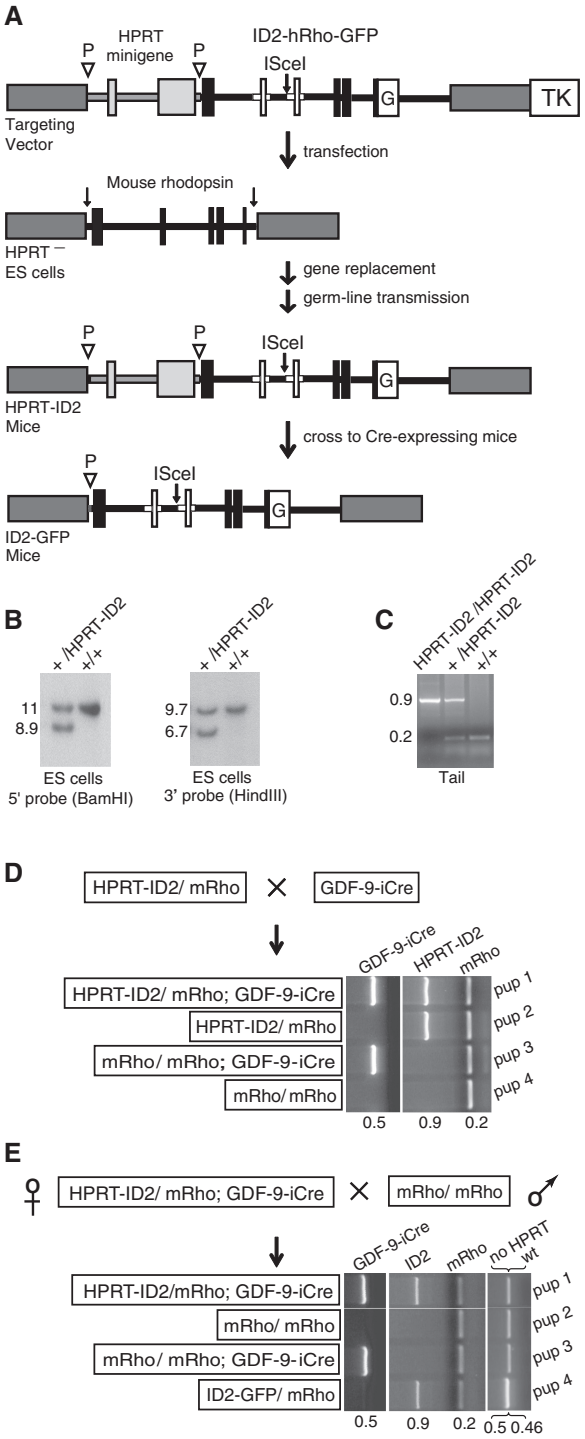

Figure 1. Generation of human rhodopsin-GFP mouse. (**A**) Strategy for replacing the mouse rhodopsin gene with the ID2-hRho-GFP gene. The mouse rhodopsin gene and flanking sequences are shown in dark gray, with exons indicated by rectangles and introns by lines. The human rhodopsin–GFP fusion gene is shown in black except for the duplicated segments containing exon 2 and the fused GFP (G) gene, which are shown in white. LoxP sites (inverted triangles marked with P) flank the HPRT minigene (light gray), which was inserted at the boundary between the human and mouse rhodopsin sequences. The 3′ boundary between human and mouse DNA is marked by a Lox511 site, which is not shown as it played no role in these experiments. (**B**) Southern blot analysis of ES cells. Restriction enzymes used to digest genomic DNA for analysis of the 5′- and 3′-ends of the modified locus are shown in parentheses, and fragment sizes are indicated in kilobases. (**C**) PCR analysis of tail DNA from HPRT-ID2 targeted mice. PCR product sizes are indicated in kb. (**D**) Breeding scheme to generate mice carrying the HPRT-ID2 and GDF-9-iCre genes. Heterozygous HPRT-ID2 mice were crossed with GDF-9-iCre mice. Examples of mice with each of the four expected gene combinations are shown. (**E**) Breeding scheme to remove the HPRT minigene. A female mouse heterozygous for both the HPRT-ID2 gene and the GDF-9-iCre transgene was crossed to a wild-type (C57BL/6) mouse. Examples of mice with four different gene combinations are shown. Pup 4 contains the ID2-hRho-GFP gene, but not the GDF-9-iCre transgene or the HPRT minigene.

create an mRNA with a termination codon spanning the junction between the two copies of exon 2, which would encode a rhodopsin fragment terminating at amino acid 177 (equivalent to Y178ter). Third, at the 5′ junction between mouse and human rhodopsin sequences in the middle of the upstream untranslated region, we inserted a minigene encoding hypoxanthine-guanine phosphoribosyl transferase (HPRT) flanked by LoxP sites to serve as a selectable marker for manipulation of ES cells. Cre-mediated removal of the marker leaves behind a single copy of LoxP, giving rise to an mRNA that is translated ~5-fold less efficiently than an mRNA lacking LoxP (26). We designed this modification to lessen the possibility that the rhodopsin fragment made in the parent mice might cause retinal degeneration on its own, interfering with our assays for DSB repair. From previous results, we knew that expression of the reduced level of human rhodopsin-GFP (as would be generated if a DSB were repaired by HR) would be readily detectable (26,27).

We generated modified mouse ES cells by gene targeting (Figure 1A) and identified clones that were properly targeted at both their 5′- and 3′-ends by Southern blotting (Figure 1B). Blastocyst injection of these modified ES cells generated chimeric mice, some of which displayed germline transmission of the modified human rhodopsin-GFP gene (Figure 1C). Offspring carrying floxed HPRT in the ID2-hRho-GFP allele (HPRT-ID2) were bred to mice with an iCre transgene driven by the GDF-9 promoter, which is expressed in the female germline (29), to generate mice that carried both genes (Figure 1D, pup 1). Female HPRT-ID2/GDF-9-iCre mice were crossed to wild-type mice and pups were analyzed by PCR to identify those that were missing HPRT (ID2-hRho-GFP) and that did not carry GDF-9-iCre (Figure 1E, pup 4). These mice were bred to homozygosity to maintain the line. For all experiments, they were crossed to wild-type mice to generate heterozygotes that carry one ID2-hRho-GFP allele and one normal mouse allele.

To verify that the ID2-hRho-GFP allele was compatible with the development and maintenance of a healthy retina, which is essential for measuring frequencies of DSB repair over time, we examined retinal sections from mice that were heterozygous for ID2-hRho-GFP. The morphology of ID2-hRho-GFP retinas was normal. In addition, the number of nuclei in the outer nuclear layer at 1 month was normal, and the rate of loss of nuclei was slight and indistinguishable from the rate in mice that expressed non-mutant hRho-GFP (Supplementary Figure S1).

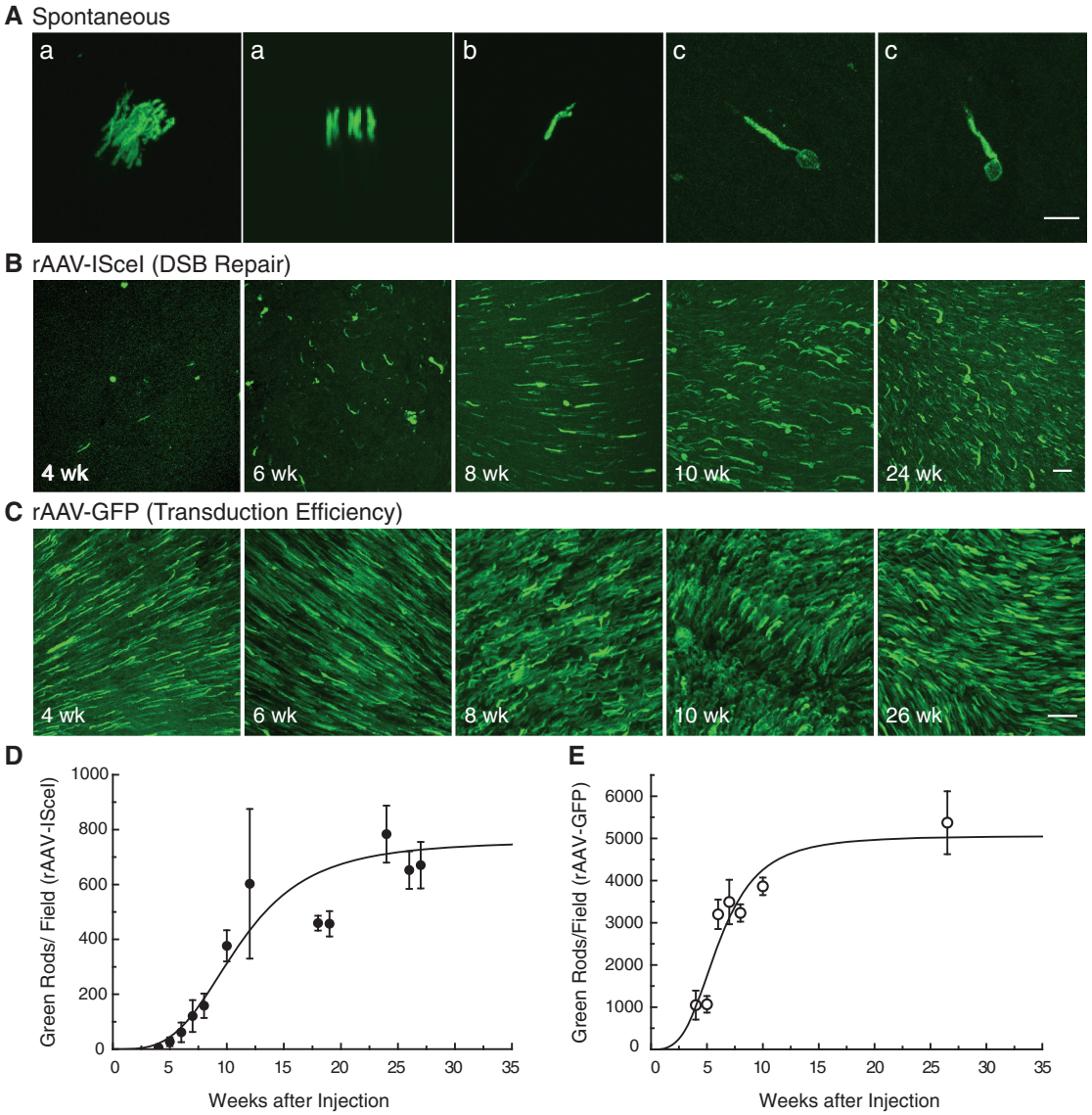

Figure 2. Fluorescent green rods in retinal whole mounts from heterozygous ID2-hRho-GFP mice. (**A**) Confocal images of retinal whole mounts from heterozygous ID2-hRho-GFP mice. (a) Images of clusters of green rods. (b) Image of rod doublets. As was typical of doublets, the two rods were closely apposed and were difficult to distinguish except by rotation of the projection angle through the image stacks. In this image the two rods are slightly separated at one end. (c) Images of individual rod cells. All images were taken at the same magnification; scale bar is 10 μm. (**B**) Confocal images of retinal whole mounts after subretinal injection of rAAV-ISceI. For retinas expressing hRho-GFP, confocal images were captured at the indicated times post injection using a ×40 objective and a ×10 eyepiece. Scale bar is 20 μm. (**C**) Confocal images of retinal whole mounts after subretinal injection of rAAV-GFP. For retinas expressing GFP, images were captured at the indicated times using a ×63 objective and a ×10 eyepiece. Scale bar is 20 μm. (**D**) Counts of fluorescent green rods after subretinal injection of rAAV-ISceI. (**E**) Counts of fluorescent green rods after subretinal injection of rAAV-GFP. For (D) and (E), counts are expressed as number of green rods per unit area (which corresponds to the size of the field observed with a ×40 objective). Error bars indicate standard deviations.

Thus, the ID2-hRho-GFP allele should serve as an acceptable marker for experiments to detect DSB repair: neither the mutant allele nor the corrected version is expected to adversely affect the lifespan of rod cells.

Spontaneous reversion of the ID2 mutation

To establish a baseline against which to measure repair of DSBs by SSA, we examined untreated retinas from ID2-hRho-GFP mice to determine the frequency with which the internal duplications spontaneously resolve into a gene structure that can express hRho-GFP. We prepared whole mounts of 27 retinas from mice at ages ranging from 4 to 52 weeks and scanned them by fluorescence microscopy to identify rods displaying GFP fluorescence, referred to here as 'green rods'. We observed a total of 360 events, for an average of 13.3 events per retina. By fluorescence and confocal microscopy, we distinguished three categories of event: tight groups of rods containing from four to more than 30 green rods per cluster (28 events); doublets of rods, the minimal cluster (200 events); and single rods (132 events) (Figure 2A). Clusters (including doublets), which account for 63% of

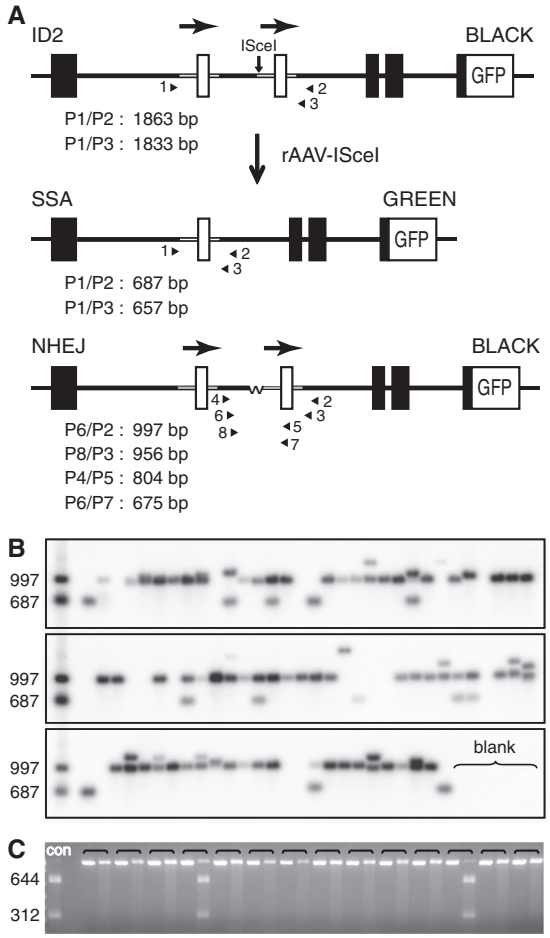

Figure 3. Analysis of SSA and NHEJ events. (**A**) Scheme for PCR analysis of SSA and NHEJ events. The duplicated copies of exon 2 along with their flanking introns are shown in white and marked by horizontal arrows. The ISceI cleavage site is indicated by a vertical arrow. Small numbered arrowheads indicate PCR primers. Primer pairs and their expected PCR fragment sizes are listed beneath the initial ID2-hRho-GFP gene and the structures of the genes resulting from SSA- and NHEJ-mediated repair of ISceI-induced DSBs. (**B**) Small-pool PCR of DNA from a single AAV-ISceI-injected retina. A mixture of primers (P1/P6/P2) was used to amplify DNA samples, and the PCR fragments were separated by gel electrophoresis and visualized by Southern blotting. Size markers for products of NHEJ (997 bp, primers P6/P2) and SSA (687 bp, primers P1/P2) are present in the first lanes of each blot. We counted bands at the position of the SSA marker as arising from SSA events, and bands at the position of the NHEJ marker and elsewhere as arising from NHEJ events (or background genomes with intact ISceI sites). Each distinct band was counted once, regardless of its intensity. (**C**) Distinguishing NHEJ events from background genomes with intact ISceI sites. Samples with bands at 997 bp were re-amplified with nested primers P8/P3, subjected to ISceI digestion, and displayed on agarose gels. The first lane shows the 644- and 312-bp bands expected for digestion of a PCR product (956 bp) with an intact ISceI site. The rest of the samples are shown in pairs, with the undigested control on the left and the ISceI-digested sample on the right. In two instances on this gel, the amplified sample was cleaved with ISceI; these samples were designated ISceI$^+$ (Table 1).

all events, presumably arose by HR during proliferation of retinal progenitor cells, which divide to generate columns of retinal neurons during differentiation of the retina (33,34). As expected since they were generated in progenitor cells, the numbers of clusters showed no age dependence over the range of observation. Surprisingly, however, the same was true for single rods, suggesting that these spontaneous events may occur much more frequently in terminally differentiated cells shortly after the last cell division than at later times in the fully developed cells. In any case, this analysis establishes that spontaneous green rods in the retinas of ID2-hRho-GFP mice are rare. Given that mouse retinas contain ~6.4 million rods (35), spontaneous events that generate green rods (13.3 per retina) occur at a frequency of $\sim 2 \times 10^{-6}$. This very low frequency defines the baseline against which to compare DSB-induced SSA events.

Repair of DSBs in the ID2-hRho-GFP gene

To induce DSBs in the target rhodopsin gene, we injected rAAV-ISceI subretinally in 3- to 4-week old ID2-hRho-GFP mice and followed the appearance of fluorescent green rods for several months by confocal microscopy. Expression of passenger genes from subretinally injected rAAV typically takes up to 3 weeks—a delay thought to be due to the slow conversion of rAAV DNA to a transcriptionally active, double-stranded form in rod cells (30). As shown in Figure 2B, green rods first appeared at ~4 weeks post-injection and continued to increase in frequency over time. To measure the efficiency of rAAV transduction, we injected rAAV-GFP and followed appearance of rods expressing GFP (Figure 2C). We calculated frequencies as the number of green rods per area observed in the ×40 objective field (230 μm × 230 μm), which contains ~23 000 rod photoreceptors (35), and plotted them as shown in Figure 2D and E. GFP expression after subretinal injection of rAAV-GFP (Figure 2E) indicates that 22% of rods were transduced by 6 months after treatment. At that time, 3.3% of rods expressed hRho-GFP (Figure 2D), indicating that 3.3/22 = 15% of transduced rods had been modified to express hRho-GFP. Thus, the frequency of green rods among transduced cells is >70 000-fold above the frequency of spontaneous green rods. Because rAAV vectors have been shown to persist and express their passenger genes robustly for at least 6 months in the mouse retina (36), the simplest explanation for the plateau in the number of events seen in Figure 2D is that by 6 months ISceI has cleaved the genome in all the rod cells where it is expressed. Those events that have not undergone repair by SSA have been repaired by mutagenic NHEJ, leading to loss of the ISceI site, an explanation confirmed by the analysis of the products presented below.

Products of ISceI-induced DSBs

We designed the ID2 target so that delivery of a DSB at the ISceI site between the duplicated segments would stimulate recombination via SSA, giving rise to green rods. In addition, we expected mutagenic NHEJ to generate alterations at the site of ISceI cleavage. To determine which of these potential products had been generated by treatment of ID2-hRho-GFP mice with rAAV-ISceI, we analyzed ISceI-resistant genomes, since both SSA and NHEJ products would lack the ISceI site. Digestion with

ISceI was carried out to remove the background of ISceI-sensitive genomes that come from non-rod cells [~22% of retinal cells (35)] and from rod cells that had not been transduced.

We subjected DNA from treated retinas to two or three cycles of ISceI digestion and PCR amplification of the region around exon 2 (Supplementary Figure S2). To enrich for the products of SSA (Figure 3A), we used primers P1/P2 in the initial round of amplification and primers P1/P3 subsequently. The 657-bp band corresponding to the putative SSA product was purified from the gel after the final cycle and cloned (Supplementary Figure S2). DNA sequence analysis revealed that the cloned DNA matched the expected product of recombination between the two copies of exon 2, as illustrated in Figure 3A. These results confirm that SSA between duplicated segments occurs in rod cells. To verify that the genomes in green rods had structures consistent with their generation by SSA, we isolated 13 individual green rods from dissociated retinas and analyzed their hRho-GFP mRNA by RT–PCR, using primers in exon 1 and GFP, as shown for eight rods in Figure 4. As authenticated by DNA sequencing, rods that expressed hRho-GFP gave a 791-bp band with one copy of exon 2, whereas rods that did not express hRho-GFP gave a 960-bp band with two copies of exon 2 (Figure 4).

To enrich for the products of NHEJ (Figure 3A), we amplified ISceI-resistant DNA using primers P4/P5 in the initial round of amplification and primers P6/P7 subsequently. To ensure that we could detect the maximum size NHEJ-induced deletions compatible with our primers (300 bp in either direction from the ISceI site), we cloned the unfractionated amplification products after the last cycle of PCR. We analyzed 128 colonies by PCR (Supplementary Figure S3). Except for the few with apparent insertions, the PCR products from these colonies seemed to have very minor changes in the size, with no obvious deletions. We obtained sequences for 37 clones. Fourteen retained the intact ISceI site, indicating that some uncleaved genomes evaded our isolation procedure. Among the remainder, 19 had small deletions ranging from 1 to 13 bp and four had insertions (Figure 5, column A). The two longer insertions, which were 42 and 48 bp, were derived from the inverted terminal repeats of rAAV. The size of the deletions, the 0–3 nt of microhomology at deletion junctions, and the proportion of insertions are all typical characteristics of NHEJ (37). Moreover, the modifications all overlap the site at which ISceI is predicted to introduce a DSB. These results confirm that ISceI cleaves rod cell genomes and that NHEJ occurs in rod cells.

In principle, ISceI-treated ID2-hRho-GFP mice could also give rise to green rods by NHEJ, if sufficient DNA sequence were deleted at the break to inactivate the upstream or downstream copy of exon 2 (889 and 457 bp, respectively). Primers P6/P7 (Figure 3A) could have detected deletions up to 300 bp on either side of the ISceI site, but uncovered no deletions that extended >50 bp into the flanking sequences. In the small-pool PCR experiments described below, primers P6/P2 could have detected a 600-bp deletion into the downstream copy of exon 2, but, once again, no significant deletions were observed in more than 200 NHEJ junctions (Figure 3B). Thus, NHEJ does not account for a significant proportion of the green rods found after ISceI cleavage.

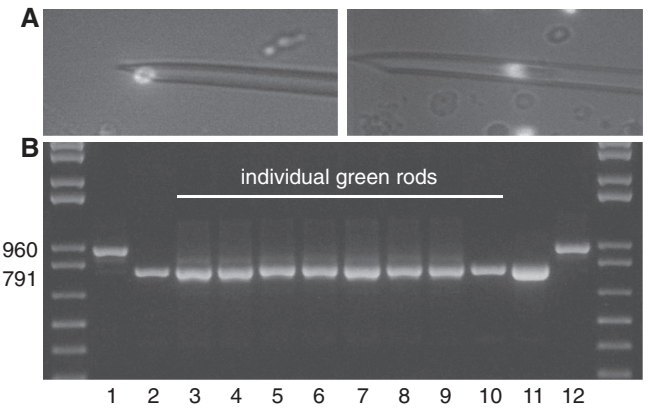

Figure 4. Analysis of individual green rods. (**A**) Fluorescence micrographs of an individual green rod cell being selected and removed using a micropipette. (**B**) PCR amplification of hRho-GFP cDNA from initial RT-PCR reactions. Lane 1, 960-bp size marker for NHEJ and background events, which contain two copies of exon 2. Lane 2, 791-bp size marker for SSA events, which contain one copy of exon 2. Lanes 3–10, PCR products from individual green rods. Lane 11, PCR product from control fluorescent rod isolated from retina of heterozygous hrhoG(H) mouse, which carries one copy of a wild-type human rhodopsin-GFP fusion gene (26). Lane 12, non-fluorescent retinal cell isolated from an rAAV-ISceI injected retina. Sequencing results confirmed that samples 3 through 10 all contain a single copy of exon 2, as expected for SSA events.

Relative frequencies of DSB repair by NHEJ and SSA

Although the above studies confirm that DSBs can be repaired by NHEJ and by the SSA pathway of HR in terminally differentiated rod cells, they do not address the issue of the relative frequencies with which these pathways repair a DSB. To measure their relative frequencies, we chose to use small-pool PCR to assess individual genomes. We isolated DNA from three retinal whole mounts that displayed large areas of green rods at 10, 12 or 24 weeks after subretinal injection of rAAV-ISceI. We extensively digested the DNA with ISceI to cleave genomes that retained the ISceI recognition sequence (i.e. genomes from cells that had not been transduced by rAAV or had not been repaired by SSA or NHEJ), and then diluted the resulting DNA so that each PCR reaction contained on average fewer than two intact genomes. We separated the PCR products (generated by a mixture of primers P1, P2 and P6) by gel electrophoresis, as shown in Figure 3B, and counted the number of bands at the position of the SSA marker (687 bp, primers P1/P2) as SSA events, and the number at the position of the NHEJ marker (997 bp, primers P6/P2) and at higher positions as presumptive NHEJ events.

Each sample with a band at the position of the NHEJ marker was re-amplified and digested with ISceI to determine whether the band was a true NHEJ event or was

derived from an intact background genome (Figure 3C). This analysis identified a small percentage of background genomes, which were eliminated from further consideration (Table 1). For several NHEJ events, we amplified the DNA and analyzed it by sequencing. As expected, bands at the position of the NHEJ marker gave small deletions, whereas slower migrating bands yielded insertions. We also reamplified several bands at the position of the SSA marker and confirmed by sequencing that they had been generated by SSA. Table 1 summarizes the data obtained from three retinas. This analysis indicates that NHEJ accounted for ~85% of DSB-repair events, whereas SSA accounted for ~15%.

Absolute frequency of NHEJ

Ultimately, the ability to use mutagenic NHEJ (and HR) for therapeutic genome editing depends on the overall efficiency with which changes can be introduced into the retina. To measure the absolute frequency of rods with NHEJ events, we isolated DNA from a retina 24 weeks after injection of rAAV-ISceI (Retina A in Table 1). We selected this retina because ~60–80% had been exposed to rAAV-ISceI, as judged by the distribution of green rods. We amplified the DNA by PCR using primers P6/P7, which does not distinguish between unaltered genomes and NHEJ-induced mutant genomes (Figure 3A). The PCR products were cloned and analyzed. Among 146 clones, we found 20 that contained NHEJ junctions (Figure 5, column B), which corresponds to 13.7% with a standard deviation of 3% expected from Poisson statistics. Since ISceI is expressed only in rod cells, which constitute 78% of retinal cells (35), the overall frequency of rod genomes with engineered NHEJ mutations is $17.6 \pm 3.8\%$ for the whole retina. Given the relative frequencies of NHEJ (85% of all events that lead to loss of the ISceI site) and SSA (15% of those events) (Table 1), we can estimate that the overall frequency of rod genomes with SSA events is about $17.6\% \times 0.15/0.85 = 3.1\%$ in this retina. Making a small adjustment (dividing by 103.1%) to account for the SSA events, which were excluded by the PCR strategy, gives absolute frequencies for this retina of ~17% of rods with NHEJ events and ~3% with SSA events.

These absolute values depend critically on the fraction of the retina that was exposed to rAAV-ISceI, which

Table 1. Small-pool PCR analysis of injected retinas

Retina[a]	PCR samples	Lanes with no bands[b]	Genomes per reaction[b]	ISceI^{+}[c]	NHEJ[d] (%)	HR[d] (%)
A1	90	15	1.8	2	76 (85)	13 (15)
A2	90	13	1.9	7	74 (84)	14 (16)
B	90	51	0.6	1	34 (83)	7 (17)
C	90	59	0.4	6	23 (82)	5 (18)

[a]Three different retinas were used. A1 and A2 are replicates of a single retina.
[b]The number of lanes that did not show a product was used to estimate the average number of intact, amplifiable genomes per reaction, using the Poisson distribution.
[c]ISceI^{+} indicates the number of samples that had upper bands that were cleavable with ISceI, indicating that they were not the products of NHEJ events.
[d]NHEJ events equal the number of distinct bands around the 997-bp marker, minus the number of ISceI^{+} samples. HR events equal the number of bands at the 687-bp marker. In neither case, have we made an attempt to correct for samples that may contain two distinct genomes that give the same size band.

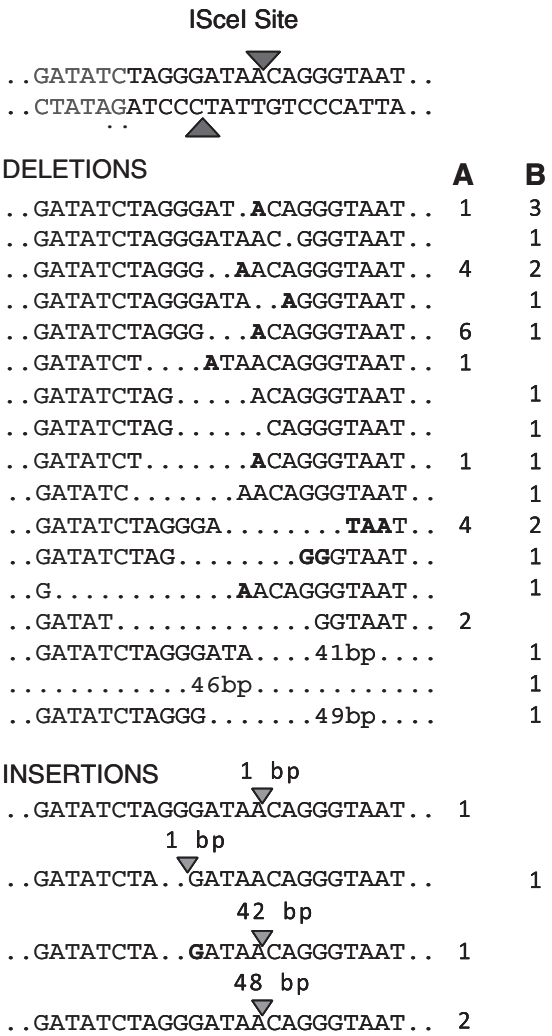

Figure 5. Sequence analysis of 43 NHEJ clones. Both DNA strands for the ISceI site are shown at the top in black with the sites of cleavage indicated by triangles on the top and bottom strand. An adjacent EcoRV site used in construction of the duplication is shown in gray. For deletions and insertions, only the top strand is shown. The column labeled A shows the results of analysis of 23 ISceI-resistant clones isolated after the treatment described in Supplementary Figure S2. The column labeled B shows the results of analysis of 20 ISceI-resistant clones isolated by screening a population of cloned PCR fragments from genomic DNA that had not been pre-digested with ISceI. The number of clones with the same sequence is shown adjacent to the sequence. Deleted nucleotides are indicated as dots. Junctional homologies for deletions are indicated by bold nucleotides and have arbitrarily been shown to the right of the deleted nucleotides. The number of inserted nucleotides is indicated above the triangles, which indicate the place in the sequence where they were inserted. The inserted sequences are: 1 bp, A; 1 bp, C; 42 bp, CCC GGCCTCAGTGAGCGAGCGAGCGCGCAGAGAGGGAGTGGC; and 48 bp, GTCGGGCGGCCTCAGTGAGCGAGCGAGCGCGCA GAGAGGGAGTGGCCA.

varies from injection to injection. We can adjust these values to allow comparisons between retinas by taking into account the area exposed to rAAV-ISceI. Since 60–80% of the area of Retina A was exposed, the adjusted frequencies per exposed portion are 21–28% for NHEJ events and 3.8–5.0% for SSA events, with the total frequency of ISceI-induced events in the range of 25–33% of rod cells in the exposed area. The value calculated for SSA events is in reasonable agreement with the frequency (3.3%) derived from the experiments shown in Figure 2B and D, which measured frequencies in exposed areas of the retina. In those experiments we also estimated that ~22% of rod cells were transduced. The similar values for transduction efficiency (22%) and proportion of modified rods in transduced areas (25–33%) suggest that the ID2-hRho-GFP gene is cleaved in virtually all rAAV-ISceI transduced rods.

DISCUSSION

Diseases that are caused by dominant alleles—like RP due to dominant rhodopsin mutations—present a special challenge for gene therapy (6). One cannot simply replace a missing function by adding in a good copy of the gene, as can be done for recessive diseases. One general therapeutic strategy for dealing with dominant mutations is to use a gene-specific damaging agent to knockout the defective gene by NHEJ or to stimulate its correction by HR (38). However, we know very little about NHEJ and HR in terminally differentiated neurons, or about the efficiency with which gene-specific damage can be induced. Using a mouse model with an internal duplication of rhodopsin exon 2 (ID2-hRho-GFP), we show here that mutations can be induced in virtually 100% of transduced rod cell neurons, with ~85% due to DSB repair by NHEJ and ~15% by the SSA subpathway of HR. These results indicate that therapeutic gene modification in rod cells is feasible.

In the experiments reported here, we designed a substrate with an internal duplication to set up a competition between DSB repair by NHEJ and SSA, in order to probe the repair capabilities of rod photoreceptors. In the absence of the duplication, as occurs in native rhodopsin alleles, and in the absence of an HR-promoting sister chromatid, which is lacking in terminally differentiated cells, mutagenic NHEJ would be expected to repair virtually all DSBs. Thus, the limit to rhodopsin mutagenesis depends on the proportion of rod cells in which DSBs can be introduced, which depends in turn on the efficiency of rod-cell transduction and on the efficiency of cleavage in transduced cells. We show here that essentially all the rod cells transduced with rAAV-ISceI acquire DSBs in the ID2-hRho-GFP target gene. This very high-cleavage efficiency is likely due to the persistence of rAAV vectors, which have been shown to express their passenger genes robustly in the mouse retina for at least 6 months (36). Although cleavage efficiency is excellent, our transduction efficiency is only ~25%. However, recent reports suggest that transduction efficiencies can be improved using other serotypes of AAV (39,40), an observation we have confirmed in our system (F. Chan, unpublished data).

The high efficiency of DSB repair by mutagenic NHEJ suggests that it could serve as the basis for strategies designed to knockout dominant rhodopsin alleles in rod cells. The key will be to design a nuclease that can cleave within the coding region of the rhodopsin gene. Over the past decade substantial progress has been made in the development of zinc-finger nucleases (ZFNs), which can be engineered to cleave specific target genes (41). ZFNs have proven exceptionally versatile, specific and selective agents for introducing gene-specific DSBs into the genomes of cultured cells and a variety of organisms (11,38,41–45). Head-to-head comparisons with ISceI, the gold standard for cleaving genomic DNA, have shown that ZFNs can cut as efficiently as ISceI (10). By designing a ZFN to cleave near the beginning of the rhodopsin gene, repair of the break by NHEJ could be used to shift the reading frame (two-thirds of the time on average) to generate a fragmentary product. Gene knockout by NHEJ repair of ZFN-induced DSBs has been used to generate several mutant cell lines and organisms (41,42). The efficient DSB-induced mutagenesis we observe in rod cells suggests that ZFN-directed gene knockout may be a promising avenue to explore as a potential therapy for RP patients with defective rhodopsin alleles.

It is no surprise that NHEJ is the primary mechanism for DSB repair in terminally differentiated rod cells, as it is in cycling mammalian cells (13). However, it is surprising that 15% of ISceI-induced DSBs in terminally differentiated rod neurons are repaired by the SSA subpathway of HR. Previous studies in cycling cells have shown that strand-invasion, the main pathway of HR, occurs predominantly in S and G2, when the sister chromatid can serve as the template for repair (20,21,25,46,47). In G1, strand invasion is blocked at the step of 5′ to 3′ resection of the ends, which is required to expose the single-stranded DNA tails that are necessary for invading an homologous duplex (13). This cell-cycle control of end resection is exerted by cyclin-dependent kinase (CDK), which mediates phosphorylation of CtIP in S and G2 to activate it for end resection (23–25). Although the strand-invasion and SSA pathways of HR differ in their downstream events, they both begin with end resection (13). Our studies in ID2-hRho-GFP mice show that end resection is robust in rod cells, occurring at 15% of DSBs. It is also extensive. To expose complementary exon-2 sequences on either side of the DSB, so that the resulting single-stranded tails can pair by SSA to bridge the break, requires that several hundred nucleotides of DNA be removed from each end. Efficient SSA in rod cells indicates that end resection is not an insurmountable barrier to the strand-invasion pathway of HR in rod cells. These results raise the possibility that repair of DSBs by HR, using an added non-mutant segment of DNA as a template for repair, might also be feasible as an approach to therapy for RP. Studies in cycling cells have shown that DSB-induced gene correction from an added DNA segment can occur at frequencies approaching 20% (11). In addition, it may be possible to improve the efficiency of HR-mediated gene editing in rod cells by knocking down

the activities of key NHEJ repair proteins, as has been done in cultured cells (48–51).

In this study, we have focused on the basic parameters of DSB repair in a specific class of neurons, the rod photoreceptors responsible for dim-light vision. We concentrated on these neurons because dominant rhodopsin mutations expressed in rod cells trigger the neurodegenerative events that cause the most common form of the hereditary blinding disease, RP. The highly efficient introduction of DSBs into rod cell genomes, coupled to their repair by mutagenic NHEJ, offers a promising approach to therapy of RP in human patients. While our measurements focus on DSB repair in rod photoreceptors, it is likely that the results can be extrapolated to DSB repair capabilities in other classes of mature neurons, which are poorly defined at present (14). Thus, this study lays the groundwork for any long-term efforts to use DSBs to edit genomes in mature neurons.

SUPPLEMENTARY DATA

Supplementary Data are available at NAR Online.

ACKNOWLEDGEMENTS

We thank Brandee Price (Baylor College of Medicine) for the suggestion to use small-pool PCR to determine the ratio of HR to NHEJ, Seok Hong Min (University of Florida) for his patience in teaching us how to do subretinal injections, Kristen Sykoudis for construction of the initial ID2 duplication, Yunfu Lin for help with the figures and Vincent Dion and members of the Wilson and Wensel groups for helpful discussions.

FUNDING

National Institutes of Health (EY11731 to J.H.W., EY07981 to T.G.W. and EY13729, EY11123, EY08571 to W.W.H); Vision Research Core Grant (EY002520); Robert A. Welch Foundation (to T.G.W.); Macular Vision Research Foundation (to W.W.H.); Research to Prevent Blindness, Inc. (to W.W.H.); Robert A. Welch Foundation (to T.G.W.). Funding for open access charge: National Institutes of Health (grant EY11731).

Conflict of interest statement. W.W.H. and the University of Florida have a financial interest in the use of AAV therapies, and own equity in a company (AGTC Inc.) that might, in the future, commercialize some aspects of this work.

REFERENCES

1. Sohocki,M.M., Daiger,S.P., Bowne,S.J., Rodriquez,J.A., Northrup,H., Heckenlively,J.R., Birch,D.G., Mintz-Hittner,H., Ruiz,R.S., Lewis,R.A. *et al.* (2001) Prevalence of mutations causing retinitis pigmentosa and other inherited retinopathies. *Hum. Mutat.*, **17**, 42–51.
2. Rivolta,C., Sharon,D., DeAngelis,M.M. and Dryja,T.P. (2002) Retinitis pigmentosa and allied diseases: numerous diseases, genes, and inheritance patterns. *Hum. Mol. Genet.*, **11**, 1219–1227.
3. Rosenfeld,P.J., Cowley,G.S., McGee,T.L., Sandberg,M.A., Berson,E.L. and Dryja,T.P. (1992) A null mutation in the rhodopsin gene causes rod photoreceptor dysfunction and autosomal recessive retinitis pigmentosa. *Nat. Genet.*, **1**, 209–213.
4. Lem,J., Krasnoperova,N.V., Calvert,P.D., Kosaras,B., Cameron,D.A., Nicolo,M., Makino,C.L. and Sidman,R.L. (1999) Morphological, physiological, and biochemical changes in rhodopsin knockout mice. *Proc. Natl. Acad. Sci. USA*, **96**, 736–741.
5. Humphries,M.M., Rancourt,D., Farrar,G.J., Kenna,P., Hazel,M., Bush,R.A., Sieving,P.A., Sheils,D.M., McNally,N., Creighton,P. *et al.* (1997) Retinopathy induced in mice by targeted disruption of the rhodopsin gene. *Nat. Genet.*, **15**, 216–219.
6. Wilson,J.H. and Wensel,T.G. (2003) The nature of dominant mutations of rhodopsin and implications for gene therapy. *Mol. Neurobiol.*, **28**, 149–158.
7. Rouet,P., Smih,F. and Jasin,M. (1994) Introduction of double-strand breaks into the genome of mouse cells by expression of a rare-cutting endonuclease. *Mol. Cell. Biol.*, **14**, 8096–8106.
8. Brenneman,M., Gimble,F.S. and Wilson,J.H. (1996) Stimulation of intrachromosomal homologous recombination in human cells by electroporation with site-specific endonucleases. *Proc. Natl Acad. Sci. USA*, **93**, 3608–3612.
9. Bibikova,M., Beumer,K., Trautman,J.K. and Carroll,D. (2003) Enhancing gene targeting with designed zinc finger nucleases. *Science*, **300**, 764.
10. Porteus,M.H. and Baltimore,D. (2003) Chimeric nucleases stimulate gene targeting in human cells. *Science*, **300**, 763.
11. Urnov,F.D., Miller,J.C., Lee,Y.L., Beausejour,C.M., Rock,J.M., Augustus,S., Jamieson,A.C., Porteus,M.H., Gregory,P.D. and Holmes,M.C. (2005) Highly efficient endogenous human gene correction using designed zinc-finger nucleases. *Nature*, **435**, 646–651.
12. Perez,E.E., Wang,J., Miller,J.C., Jouvenot,Y., Kim,K.A., Liu,O., Wang,N., Lee,G., Bartsevich,V.V., Lee,Y.L. *et al.* (2008) Establishment of HIV-1 resistance in CD4+ T cells by genome editing using zinc-finger nucleases. *Nat. Biotechnol.*, **26**, 808–816.
13. Kass,E.M. and Jasin,M. (2010) Collaboration and competition between DNA double-strand break repair pathways. *FEBS Lett.*, **584**, 3703–3708.
14. McKinnon,P.J. (2009) DNA repair deficiency and neurological disease. *Nat. Rev. Neurosci.*, **10**, 100–112.
15. Lee,Y. and McKinnon,P.J. (2007) Responding to DNA double strand breaks in the nervous system. *Neuroscience*, **145**, 1365–1374.
16. Abner,C.W. and McKinnon,P.J. (2004) The DNA double-strand break response in the nervous system. *DNA Repair (Amst)*, **3**, 1141–1147.
17. Rass,U., Ahel,I. and West,S.C. (2007) Defective DNA repair and neurodegenerative disease. *Cell*, **130**, 991–1004.
18. Ren,K. and Pena de Ortiz,S. (2002) Non-homologous DNA end joining in the mature rat brain. *J. Neurochem.*, **80**, 949–959.
19. Sharma,S. (2007) Age-related nonhomologous end joining activity in rat neurons. *Brain Res. Bull.*, **73**, 48–54.
20. Wyman,C. and Kanaar,R. (2006) DNA double-strand break repair: all's well that ends well. *Annu. Rev. Genet.*, **40**, 363–383.
21. Rothkamm,K., Kruger,I., Thompson,L.H. and Lobrich,M. (2003) Pathways of DNA double-strand break repair during the mammalian cell cycle. *Mol. Cell. Biol.*, **23**, 5706–5715.
22. Takata,M., Sasaki,M.S., Sonoda,E., Morrison,C., Hashimoto,M., Utsumi,H., Yamaguchi-Iwai,Y., Shinohara,A. and Takeda,S. (1998) Homologous recombination and non-homologous end-joining pathways of DNA double-strand break repair have overlapping roles in the maintenance of chromosomal integrity in vertebrate cells. *EMBO J.*, **17**, 5497–5508.
23. Sartori,A.A., Lukas,C., Coates,J., Mistrik,M., Fu,S., Bartek,J., Baer,R., Lukas,J. and Jackson,S.P. (2007) Human CtIP promotes DNA end resection. *Nature*, **450**, 509–514.
24. Huertas,P. and Jackson,S.P. (2009) Human CtIP mediates cell cycle control of DNA end resection and double strand break repair. *J. Biol. Chem.*, **284**, 9558–9565.

25. Ira,G., Pellicioli,A., Balijja,A., Wang,X., Fiorani,S., Carotenuto,W., Liberi,G., Bressan,D., Wan,L., Hollingsworth,N.M. *et al.* (2004) DNA end resection, homologous recombination and DNA damage checkpoint activation require CDK1. *Nature*, **431**, 1011–1017.
26. Chan,F., Bradley,A., Wensel,T.G. and Wilson,J.H. (2004) Knock-in human rhodopsin-GFP fusions as mouse models for human disease and targets for gene therapy. *Proc. Natl Acad. Sci. USA*, **101**, 9109–9114.
27. Wensel,T.G., Gross,A.K., Chan,F., Sykoudis,K. and Wilson,J.H. (2005) Rhodopsin-EGFP knock-ins for imaging quantal gene alterations. *Vision Res.*, **45**, 3445–3453.
28. Zheng,B., Sage,M., Sheppeard,E.A., Jurecic,V. and Bradley,A. (2000) Engineering mouse chromosomes with Cre-loxP: range, efficiency, and somatic applications. *Mol. Cell. Biol.*, **20**, 648–655.
29. Lan,Z.J., Xu,X. and Cooney,A.J. (2004) Differential oocyte-specific expression of Cre recombinase activity in GDF-9-iCre, Zp3cre, and Msx2Cre transgenic mice. *Biol. Reprod.*, **71**, 1469–1474.
30. Flannery,J.G., Zolotukhin,S., Vaquero,M.I., LaVail,M.M., Muzyczka,N. and Hauswirth,W.W. (1997) Efficient photoreceptor-targeted gene expression in vivo by recombinant adeno-associated virus. *Proc. Natl Acad. Sci. USA*, **94**, 6916–6921.
31. Pang,J.J., Chang,B., Kumar,A., Nusinowitz,S., Noorwez,S.M., Li,J., Rani,A., Foster,T.C., Chiodo,V.A., Doyle,T. *et al.* (2006) Gene therapy restores vision-dependent behavior as well as retinal structure and function in a mouse model of RPE65 Leber congenital amaurosis. *Mol. Ther.*, **13**, 565–572.
32. Lolley,R.N., Lee,R.H., Chase,D.G. and Racz,E. (1986) Rod photoreceptor cells dissociated from mature mice retinas. *Invest. Ophthalmol. Vis. Sci.*, **27**, 285–295.
33. Turner,D.L., Snyder,E.Y. and Cepko,C.L. (1990) Lineage-independent determination of cell type in the embryonic mouse retina. *Neuron*, **4**, 833–845.
34. Morrow,E.M., Furukawa,T. and Cepko,C.L. (1998) Vertebrate photoreceptor cell development and disease. *Trends Cell Biol.*, **8**, 353–358.
35. Jeon,C.J., Strettoi,E. and Masland,R.H. (1998) The major cell populations of the mouse retina. *J. Neurosci.*, **18**, 8936–8946.
36. Mao,H., Thomas,J. Jr, Schwein,A., Shabashvili,A., Hauswirth,W.W., Gorbatyuk,M.S. and Lewin,A. (2011) AAV Delivery of Wild-Type Rhodopsin Preserves Retinal Function in a Mouse Model of Autosomal Dominant Retinitis Pigmentosa. *Hum. Gene Ther.*, PMID 21126223 [Epub ahead of print, 7 March 2011].
37. Roth,D.B. and Wilson,J.H. (1986) Nonhomologous recombination in mammalian cells: role for short sequence homologies in the joining reaction. *Mol. Cell. Biol.*, **6**, 4295–4304.
38. Wilson,J.H. (2008) Knockout punches with a fistful of zinc fingers. *Proc. Natl Acad. Sci. USA*, **105**, 5653–5654.
39. Allocca,M., Mussolino,C., Garcia-Hoyos,M., Sanges,D., Iodice,C., Petrillo,M., Vandenberghe,L.H., Wilson,J.M., Marigo,V., Surace,E.M. *et al.* (2007) Novel adeno-associated virus serotypes efficiently transduce murine photoreceptors. *J. Virol.*, **81**, 11372–11380.
40. Petrs-Silva,H., Dinculescu,A., Li,Q., Min,S.H., Chiodo,V., Pang,J.J., Zhong,L., Zolotukhin,S., Srivastava,A., Lewin,A.S. *et al.* (2009) High-efficiency transduction of the mouse retina by tyrosine-mutant AAV serotype vectors. *Mol. Ther.*, **17**, 463–471.
41. Urnov,F.D., Rebar,E.J., Holmes,M.C., Zhang,H.S. and Gregory,P.D. Genome editing with engineered zinc finger nucleases. *Nat. Rev. Genet.*, **11**, 636–646.
42. Santiago,Y., Chan,E., Liu,P.Q., Orlando,S., Zhang,L., Urnov,F.D., Holmes,M.C., Guschin,D., Waite,A., Miller,J.C. *et al.* (2008) Targeted gene knockout in mammalian cells by using engineered zinc-finger nucleases. *Proc. Natl Acad. Sci. USA*, **105**, 5809–5814.
43. Carroll,D. (2008) Progress and prospects: zinc-finger nucleases as gene therapy agents. *Gene Ther.*, **15**, 1463–1468.
44. Meyer,M., de Angelis,M.H., Wurst,W. and Kuhn,R. Gene targeting by homologous recombination in mouse zygotes mediated by zinc-finger nucleases. *Proc. Natl Acad. Sci. USA*, **107**, 15022–15026.
45. Geurts,A.M. and Moreno,C. Zinc-finger nucleases: new strategies to target the rat genome. *Clin. Sci. (Lond)*, **119**, 303–311.
46. Lieber,M.R. (2008) The mechanism of human nonhomologous DNA end joining. *J. Biol. Chem.*, **283**, 1–5.
47. Aylon,Y., Liefshitz,B. and Kupiec,M. (2004) The CDK regulates repair of double-strand breaks by homologous recombination during the cell cycle. *EMBO J.*, **23**, 4868–4875.
48. Clikeman,J.A., Khalsa,G.J., Barton,S.L. and Nickoloff,J.A. (2001) Homologous recombinational repair of double-strand breaks in yeast is enhanced by MAT heterozygosity through yKU-dependent and -independent mechanisms. *Genetics*, **157**, 579–589.
49. Allen,C., Kurimasa,A., Brenneman,M.A., Chen,D.J. and Nickoloff,J.A. (2002) DNA-dependent protein kinase suppresses double-strand break-induced and spontaneous homologous recombination. *Proc. Natl Acad. Sci. USA*, **99**, 3758–3763.
50. Pierce,A.J., Hu,P., Han,M., Ellis,N. and Jasin,M. (2001) Ku DNA end-binding protein modulates homologous repair of double-strand breaks in mammalian cells. *Genes Dev.*, **15**, 3237–3242.
51. Delacote,F., Han,M., Stamato,T.D., Jasin,M. and Lopez,B.S. (2002) An xrcc4 defect or Wortmannin stimulates homologous recombination specifically induced by double-strand breaks in mammalian cells. *Nucleic Acids Res.*, **30**, 3454–3463.